Peer reviewed version

License (if available):
Other

Link to published version (if available):
10.1021/acs.macromol.9b00088

Link to publication record in Explore Bristol Research
PDF-document

University of Bristol - Explore Bristol Research
General rights

Nanostructured Bimetallic Block Copolymers as Precursors to Magnetic FePt Nanoparticles

Sze-Chun Yiu,[‡a,b,d] Adam Nunns,[‡b] Cheuk-Lam Ho,*[a,d] Jenner Ho-Loong Ngai,[d] Zhengong Meng,*[d] Guijun Li,[e] Jessica Gwyther,[b] George R. Whittell,[b] Ian Manners*[b,c] and Wai-Yeung Wong*[a,d]

[a] *Department of Applied Biology and Chemical Technology, The Hong Kong Polytechnic University, Hung Hom, Hong Kong, P. R. China*
E-mail: cheuk-lam.ho@polyu.edu.hk; wai-yeung.wong@polyu.edu.hk
[b] *School of Chemistry, University of Bristol, BS8 1TS, Bristol, UK*
E-mail: ian.manners@bristol.ac.uk
[c] *Department of Chemistry, University of Victoria, BC V8W 3V6, Canada*
E-mail: imanners@uvic.ca
[d] *Institute of Molecular Functional Materials and Department of Chemistry, Hong Kong Baptist University, Waterloo Road, Kowloon Tong, Hong Kong, P. R. China; HKBU Institute of Research and Continuing Education, Shenzhen Virtual University Park, Shenzhen, 518057, P. R. China*
[e] *Department of Applied Physics, The Hong Kong Polytechnic University, Hung Hom, Hong Kong, P. R. China.*

[‡]*These authors contributed equally.*

Nanostructured Bimetallic Block Copolymers as Precursors to Magnetic FePt Nanoparticles

Sze-Chun Yiu, Adam Nunns, Cheuk-Lam Ho, Jenner Ho-Loong Ngai, Zhengong Meng, Guijun Li, Jessica Gwyther, George R. Whittell, Ian Manners and Wai-Yeung Wong
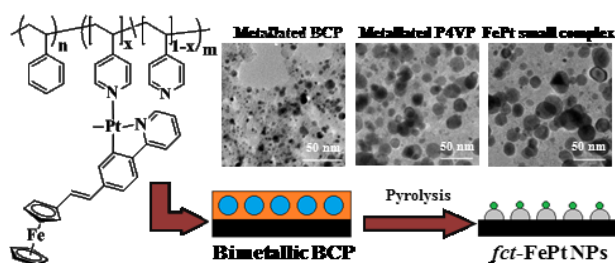
The use of a bimetallic block copolymer (BCP) as a precursor to ferromagnetic FePt nanoparticles (NPs) has been studied. The use of a phase-separated BCP rather than alternative precursors (metalated P4VP homopolymer and molecular organometallic complex) was shown to be important, giving rise to a smaller average NP size and a close to stoichiometric 1:1 Fe:Pt ratio.

ABSTRACT

Phase-separated block copolymers (BCPs) that function as precursors to arrays of FePt nanoparticles (NPs) is of potential interest for the creation of media for the next generation high-density magnetic data storage devices. A series of bimetallic BCPs has been synthesized by incorporating a complex containing Fe and Pt centers into the coordinating block of four different poly(styrene-*b*-4-vinylpyridine)s (PS-*b*-P4VPs, **P1−P4**). To facilitate phase-separation for the resulting metalated BCPs (**PM1−PM4**), a loading of the FePt-bimetallic complex corresponding to ca. 20% was used. The bulk and thin film self-assembly of these BCPs were studied by transmission electron microscopy (TEM) and atomic force microscopy (AFM), respectively. The spherical and cylindrical morphologies observed for the metalated BCPs corresponded to those observed for the metal-free BCPs. The products from the pyrolysis of the BCPs in bulk were also characterized by TEM, powder X-ray diffraction (PXRD), and energy-dispersive X-ray spectroscopy (EDX), which indicated that the FePt nanoparticles (NPs) formed exist as a *fct* phase with average particle sizes of ca. 4–8 nm within a carbonaceous matrix. A comparison of the pyrolysis behavior of the metalated BCP (**PM3**), the metalated P4VP homopolymer (**PM5**), and the molecular model organometallic complex, revealed the importance of using a nanostructured BCP approach for the synthesis of ferromagnetic FePt NPs with a smaller average NP size and a close to 1:1 Fe:Pt stoichiometric ratio.

INTRODUCTION

The development of metal-containing polymers has rapidly expanded over the past two decades,[1-6] and they have been successfully utilized, for example, as stimuli-responsive materials,[7-9] in energy conversion and storage[10-12] and as precursors of nanomaterials.[13-17] To enrich the potential functions of metallopolymers, nanostructured materials are under intensive investigation for various applications.[18-22] In general, a top-down approach is the most direct method to transfer patterns to the underlying polymers by masks or molds.[23-24] In contrast, the bottom-up approach, such as block copolymers (BCPs) lithography, relies on the intrinsic self-assembling ability of metalloblock copolymers to generate hierarchical structures. This approach has demonstrated the possibility of employing the metalloblock copolymer as lithographic hard mask to fabricate the cobalt magnetic dot arrays.[25] This approach has also shown potential for the creation of nanoparticle (NP) arrays generated by the metalated BCPs themselves due to the spatial control of metal moieties within nanometer size domains.[26-27] Hence, it allows the straightforward utilization of metallopolymers as the precursor to metal/carbon nanocomposites, and offers the desirable potential to confine the metallic/metal oxide NPs within an ordered structure on the nanometer scale. To achieve a useful morphology, a metalloblock copolymer is usually employed with sufficiently low miscibility between the blocks and high molar mass.[28] Following appropriate post-annealing procedures, this templating method has been useful for the fabrication of catalytic and magnetic nanopatterned materials.[29-32]

4

Among the metal-containing BCPs, poly(styrene-*b*-ferrocenylethylmethylsilane) (PS-*b*-PFEMS), an iron-containing BCP, has been studied extensively in both bulk and thin film self-assembly, where the immiscible blocks phase-separate into various morphologies depending on the relative volume fraction of blocks.[33] Ordered hexagonally-packed arrays of iron domains embedded in PS matrix have been realized in the literature.[30, 34] Furthermore, iron NPs (i.e. ~ 6.5 nm average size) in a C/SiC matrix could be obtained after pyrolysis. While the current work described in this manuscript was in progress, the formation of FeRu NPs for potential catalytic applications from the pyrolysis of a BCP containing Fe and Ru was described.[35] Cobalt-based nanomaterials have also been accessed using BCPs with cobalt-carbonyl clusters attached to ethynyl units[36-38] or half-sandwich cobaltocenium/ (η^5-cyclopentadienyl)(η^4-cyclobutadiene)cobalt moieties.[16, 39-40] Nanostructuring of the BCP through cylindrical domain formation has been shown to alter the magnetic properties of the resulting cobalt NPs.[38] In addition, Pd-pincer complexes have been introduced to poly(styrene-*b*-2-vinylpyridine) (PS-*b*-P2VP) *via* either coordination or through stacking interactions leading to morphological transitions[41] and the formation of disk-shaped Pd NP aggregates organized into ordered hierarchical arrays.[42]

Recently, L1$_0$ phase FePt alloy NP has received much attention due to its high magnetic anisotropic constant (i.e. 7×10^7 erg/cc) and high chemical stability relative to other hard magnets.[43-45] In addition, both *fcc*- and *fct*-FePt NPs have shown to exhibit a durable and enhanced electrocatalytic oxidation and reduction, which potentially serve as promising candidates in fuel

cells.[46-47] With novel device architectures (i.e. bit-patterned media (BPM) and energy-assisted magnetic recording), it is possible to reach an areal density of magnetic FePt NPs up to several Tbytes/in^2 for commercial applications.[48] In 2008, our groups and our collaborators employed electron beam lithography (EBL) with polyferroplatinyne polymer precursors to produce arrays of NPs microbars (ca. 1.0 × 10 μm^2) with no observable aggregation of FePt NPs.[49] Such aggregation suppression was postulated to be a consequence of the surrounding carbonaceous matrix. To further develop a low-cost large area fabrication pathway, nanoimprint lithography (NIL) was then employed to optimize the one-step pyrolysis of a polyferroplatinyne polymer.[23, 50-51] Depending on the patterns of the imprint mold, both line and dot arrays of NPs can be produced. A high coercivity up to 3.6 T of FePt NPs was also recorded.[50] However, scaling down the feature size of NPs in mold to sub-20 nm is still a problem due to the tribological phenomena in the interface between the mold/substrate and polymers.[52] To produce well-defined arrays of tiny bits of FePt NPs over large areas, BCP self-assembly offers an alternative templating method to scale down the highly dense bits in the bottom-up method. BCPs have been employed as a template to incorporate metal precursors or as-synthesized NPs to produce homogeneous highly ordered nanostructured patterns. Metal salts, molecular organometallic precursors, or magnetic NPs can be incorporated to BCPs before self-assembly to produce desired functional BCPs, where coating of oligomeric[53-54] or organic ligands[55] on NPs may be required in order to induce hydrophobic/hydrophilic interactions that favor the formation with one type of BCP nanodomain.

However, significant drawbacks including cross-linking, uncontrolled NP aggregation, and deviations from the desired stoichiometry for Fe and Pt atoms may exist if individual metal salts[56] or molecular organometallic species[57] are used to produce bimetallic NPs. The use of single bimetallic precursors was proposed.[58-59] Self-assembly of bimetallic BCPs is expected to be a promising and possible solution to direct and confine the metal precursors in one of the BCP domains and to obtain metallic NPs of low size dispersity after direct pyrolysis.[60-62] Up to now, the use of a single bimetallic BCP to synthesize FePt NPs has not been reported. Herein, we describe the synthesis of a series of bimetallic BCPs by coordinating a specifically designed FePt bimetallic complex into the nitrogen donor segment of PS-*b*-P4VP. Morphological characterization and pyrolysis studies were performed on phase-separated self-assembled materials in both bulk and in thin films in order to investigate the potential of our approach to prepare arrays of FePt NPs. The potential of the concept of the formation of large area of FePt NPs by solely using a phase-separated thin film of a bimetallic-containing BCP is captured in Figure 1.[30]
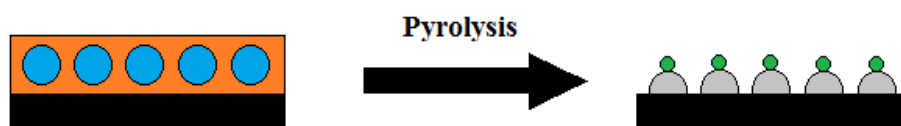
Figure 1. Schematic diagram of an idealized pyrolysis procedure (Orange: complementary matrix-forming metal-free block; Blue: FePt bimetallic complexes within spherical nano-domains; Green: FePt NPs embedded in a grey carbonaceous material). For an analogous process see Figure 4 of ref 27 for the case of Fe NPs.

EXPERIMENTAL SECTION

Materials. Samples of PS-*b*-P4VP and P4VP homopolymer, with molecular weight

characteristics shown in Table 1, were purchased from Polymer Source and used as received.

Potassium tetrachloroplatinate(II), tetrakis(triphenylphosphine)palladium(0), 2-bromopyridine,

n-BuLi (1.6 M solution in cylcohexane), tetramethyltin, tributyltin chloride and the other

chemicals mentioned in the experimental part were purchased from Aldrich, Tokyo Chemical

Industry Co. and Alfa Aesar. Solvents were either dried by standard procedures or purchased from

Aldrich. 2-(Tributylstannyl)pyridine, *cis*-dichlorobis(dimethyl sulfoxide)platinum(II),

cis-dimethylbis(dimethyl sulfoxide)platinum(II) and (*E*)-1-[2-(4-Bromophenyl)vinyl]ferrocene **(1)**

were prepared as described in the literature.[63-66] Unless otherwise stated, all reactions were carried

out under nitrogen with standard Schlenk techniques. Reactions were monitored by thin layer

chromatography (TLC) with Merck pre-coated aluminum plates, whereas silica gel for column

chromatography was purchased from Merck and used directly for product separation and

purification.

Table 1. Molecular weight and volume fraction data of neat PS-*b*-P4VPs and P4VP.

	M_n(PS)–M_n(P4VP) (kg/mol) [a]	PDI[a]	ϕ_{P4VP} [b]	n:m
P1	33.0–8.0	1.10	0.186	316:76
P2	48.0–11.0	1.13	0.178	459:104
P3	54.0–6.5	1.08	0.102	517:62
P4	120.0–20.0	1.18	0.136	1148:190
P4VP (P5)	6.5	1.09	-	-

[a] Provided by the commercial supplier, Polymer Source Inc.

Preparation of AFM thin films and TEM bulk films. Samples for AFM imaging were prepared by spin-coating (3000 rpm, 60–70 s) from 0.6 wt% chloroform solution of BCP on silicon substrates. TEM samples were prepared by drop-casting chloroform solution (50 mg/mL) on glass slide and thermally annealed under vacuum at 180 °C for four days, followed by liquid nitrogen quenching. Ultra-thin sections (60–80 nm) of the bulk films were microtomed and imaged by TEM.

Instrumentation. ^{1}H and ^{13}C NMR spectra were obtained from Varian 400 and 500 MHz spectrometers. IR analysis was performed with Perkin-Elmer Spectrum Two IR spectrometer equipped with attenuated total reflectance (ATR) FT-IR accessary. Mass analysis was performed with Agilent 6540 Liquid Chromatography – Electrospray Ionization Quadrupole-Time-of-Flight Mass Spectrometer, using methanol and acetonitrile as eluent. Thermogravimetric analysis (TGA) was performed with TA instruments Q500 using platinum sample pan scanning from 25 to 800 °C at a heating rate of 10 °C/min under nitrogen. Spin-coating of the thin film was performed by a Laurell WS-400B-6NPP-LITE spin coater under an argon purge. Silicon wafers were purchased from Wafer World, Inc, and rinsed with dichloromethane (CH_2Cl_2), tetrahydrofuran (THF), acetone and deionized water before use. AFM was carried out in the tapping mode with 10 nm wide cantilevers (Nunano, Scout 350) using a Nanoscope 3D microscope. TEM was performed on

a Philips Tecnai G2 20 S-TWIN, operating with a tungsten filament at 200 kV. FePt NPs were

prepared by direct pyrolysis of polymers in 5% H_2/Ar, in which the samples were placed in a

ceramic boat inside a quartz tube furnace. The tube was then purged with 5% H_2/Ar for an hour

and heated to 800 °C from 50 °C in an hour. The temperature was held at 800 °C for 1 h, followed

by cooling to room temperature over 2 h. The black powders were then collected. A little amount

of the powder was suspended in ethanol and sonicated for an hour. The suspension was then

drop-casted on the copper grid coated with carbon film. The sample was air dried and imaged by

TEM. Composition analysis was performed by EDX on fully embedded EDAX detectors within

TEM. The test area was between 500 x 500 to 1000 x 1000 nm^2. Structural characterization was

performed by PXRD on a Bruker D8 machine equipped with Cu $K_{\alpha1}$ (λ = 540 nm, 40 kV, dan 30

mA). The magnetic properties were measured by the Physical Property Measurement System

(PPMS) at 300 K.

Synthesis of 2-[4-[(1*E*)-2-Ferrocenylethenyl]phenyl]pyridine (2). To 50 mL dry toluene, **1**

(3.00 g, 8.2 mmol) and 2-(tributylstannyl)pyridine (3.61 g, 10.0 mmol) were added. A catalytic

amount of Pd(PPh$_3$)$_4$ was then introduced. The mixture was refluxed at 110 °C for 2 days. The

mixture was purified through a wet column with silica gel eluting with hexane and ethyl acetate

(6:1, v/v). A red orange solid was obtained in 76% yield (2.27 g). ^{1}H NMR (400 MHz, CDCl$_3$): δ

8.70 (d, *J* = 4.8 Hz, 1H, Ar), 7.99 (d, *J* = 8.3 Hz, 2H, Ar), 7.75 (d, *J* = 5.0 Hz, 2H, Ar), 7.54 (d, *J* =

8.3 Hz, 2H, Ar), 7.22 (m, 2H, Ar), 6.97 (d, J = 16.3 Hz, 1H, **CH**=CH), 6.75 (d, J = 16.3 Hz, 1H,

CH=C**H**), 4.49 (t, J = 3.7 Hz, 2H, ferrocenyl), 4.31 (t, J = 3.7 Hz, 2H, ferrocenyl), 4.16 (s, 5H,

ferrocenyl) ppm. ^{13}C NMR (100 MHz, CDCl$_3$): δ = 157.25, 149.85, 138.36, 137.34, 136.85,

127.98, 127.28, 126.27, 125.65, 122.06, 120.37, 83.35, 69.40, 69.32, 67.12 ppm. HRMS (ESI-MS,

m/z): [M+H]$^+$ 366.0945; calcd for C$_{23}$H$_{20}$FeN (M+H) 366.0945.

Synthesis of 3. *cis*-Pt(CH$_3$)$_2$(DMSO)$_2$ (0.40 g, 1.0 mmol) was dissolved in acetone and **2**

(0.38 g, 1.0 mmol) was added. The reaction mixture was refluxed at 50 °C overnight. The reaction

mixture was then precipitated in hexane for several times and the formed red orange solid was

dried *in vacuo* in 86% yield (0.59 g). ^{1}H NMR (400 MHz, CDCl$_3$): δ 9.72 (d, J = 5.9 Hz, 1H, Ar),

7.78 (m, 3H, Ar), 7.60 (d, J = 8.1 Hz, 1H, Ar), 7.24 (d, J = 8.1 Hz, 1H, Ar), 7.24 (t, J = 13.0 Hz,

1H, Ar), 6.94 (d, J = 16.0 Hz, 1H, **CH**=CH), 6.76 (d, J = 16.0 Hz, 1H, CH=C**H**), 4.49 (t, J = 3.5

Hz, 2H, ferrocenyl), 4.29 (t, J = 3.5 Hz, 2H, ferrocenyl), 4.14 (s, 5H, ferrocenyl), 3.25 (s, J_{Pt-H} =

16.6 Hz, 6H, SO((CH$_3$)$_2$), 0.78 (s, J_{Pt-H} = 81.9 Hz, 3H, **CH**$_3$) ppm. HRMS (MALDI-TOF, m/z):

[M-H]$^+$ 651.0724; calcd for C$_{26}$H$_{26}$FeNOPtS (M-H) 651.0732.

Synthesis of 4. 3 (0.50 g, 0.8 mmol) was dissolved in CHCl$_3$ (10 mL) and pyridine (0.31 g,

4.0 mmol) was added. The reaction mixture was stirred overnight and precipitated from hexane to

get the target compound as a red solid in 80% yield (0.40 g). ^{1}H NMR (400 MHz, CDCl$_3$): δ 8.87

(d, J = 5.0 Hz, 2H, py), 7.79 (m, 5H, Ar), 7.51 (m, 3H, Ar), 7.16 (m, 1H, Ar), 6.94 (d, J = 16.2 Hz, 2H, Ar and C**H**=CH), 6.75 (d, J = 16.2 Hz, 1H, CH=C**H**), 4.50 (t, J = 3.6 Hz, 2H, ferrocenyl), 4.28 (t, J = 3.6 Hz, 2H, ferrocenyl), 4.14 (s, 5H, ferrocenyl) , 0.92 (m, 3H, C**H**$_3$) ppm. HRMS (MALDI-TOF, m/z): [M-H]$^+$ 652.1010; calcd for C$_{29}$H$_{25}$FeN$_2$Pt (M-H) 652.1019.

Synthesis of PM1-PM5.

P1 (0.10 g, 2.4 µmol) was dissolved in CHCl$_3$ and **3** (0.024 g, 36.8 µmol, 20% of the pyridine unit) was then added. The reaction mixture was stirred overnight and precipitated in diethyl ether for three times. The polymeric product was dried under vacuum at 40 °C for two days and isolated as an orange solid in 56% yield (0.069 g). ^{1}H NMR (400 MHz, CD$_2$Cl$_2$): δ 8.55–8.07 (br, Ph and uncomplexed 2,6-Py), 7.97–7.40 (br, Ph), 7.23–6.13 (br, Ph), 4.61–3.93 (b, ferrocenyl), 2.40–0.60 (br, aliphatic -C**H**C**H**$_2$-).

P2 (0.10 g, 1.7 µmol) was dissolved in CHCl$_3$ and **3** (0.022 g, 33.9 µmol, 20% of the pyridine unit) was then added. The polymer was prepared by a procedure identical to that for **P1** and isolated as an orange solid in 70% yield (0.080 g). ^{1}H NMR (400 MHz, CD$_2$Cl$_2$): δ 8.49–8.06 (br, Ph and uncomplexed 2,6-Py), 7.96–7.41 (br, Ph), 7.30–6.24 (br, Ph), 4.60–4.00 (b, ferrocenyl), 2.35–0.61 (br, aliphatic -C**H**C**H**$_2$-).

P3 (0.10 g, 1.7 µmol) was dissolved in CHCl$_3$ and **3** (0.013 g, 20.5 µmol, 20% of the pyridine unit) was then added. The polymer was prepared by a procedure identical to that for **P1** and

isolated as an orange solid in 59% yield (0.065 g). ^{1}H NMR (400 MHz, CD$_2$Cl$_2$): δ 8.58–8.10 (br, Ph and uncomplexed 2,6-Py), 8.01–7.63 (br, Ph), 7.49–6.00 (br, Ph), 4.61–3.90 (b, ferrocenyl), 2.36–0.46 (br, aliphatic -CHCH$_2$-).

P4 (0.10 g, 0.7 µmol) was dissolved in CHCl$_3$ and **3** (0.018 g, 27 µmol, 20% of the pyridine unit) was then added. The polymer was prepared by a procedure identical to that for **P1** and isolated as an orange solid in 52% yield (0.061 g). ^{1}H NMR (400 MHz, CD$_2$Cl$_2$): δ 8.56–8.05 (br, Ph and uncomplexed 2,6-Py), 7.88–7.41 (br, Ph), 7.27–6.29 (br, Ph), 4.51–4.01 (b, ferrocenyl), 2.38–0.81 (br, aliphatic -CHCH$_2$-).

**P5** (0.10 g, 153.8 µmol) was dissolved in CHCl$_3$ and **3** (0.124 g, 190.8 µmol, 20% of the pyridine unit) was then added. The polymer was prepared by a procedure identical to that for **P1** and isolated as an orange solid in 60% yield (0.133 g). ^{1}H NMR (400 MHz, CD$_2$Cl$_2$): δ 8.54–5.99 (br, Ar, complexed and uncomplexed 2,6-Py), 4.63–3.93 (b, ferrocenyl), 2.70–0.74 (br, aliphatic -CHCH$_2$-).

RESULTS AND DISCUSSION

Synthesis and structural characterization of PM1−PM4. The ferrocene-containing C^N ligand **2** was synthesized by Stille coupling of **1** and 2-(tributylstannyl)pyridine, whereas *cis*-Pt(CH$_3$)$_2$(DMSO)$_2$ was prepared by reacting tetramethyltin with potassium tetrachloroplatinate(II) (Scheme 1).[63-65] **3** was then obtained readily by cyclometalation of

cis-Pt(CH$_3$)$_2$(DMSO)$_2$ with the C^N ligand. The weak DMSO donor was then replaced by either

pyridine or the pyridine units in PS-*b*-P4VP to give **4** and **PM1−PM4**, respectively. The polymers

can be obtained simply by precipitation from diethyl ether as orange powders in quantitative

yields. Approximately 20% complexation of 4-vinylpyridine with bimetallic complexes along the

polymer backbone was used in this study to preserve the desired morphologies, namely spheres

and cylinders (for an explanation of the rationale for the target loading, see the following section).
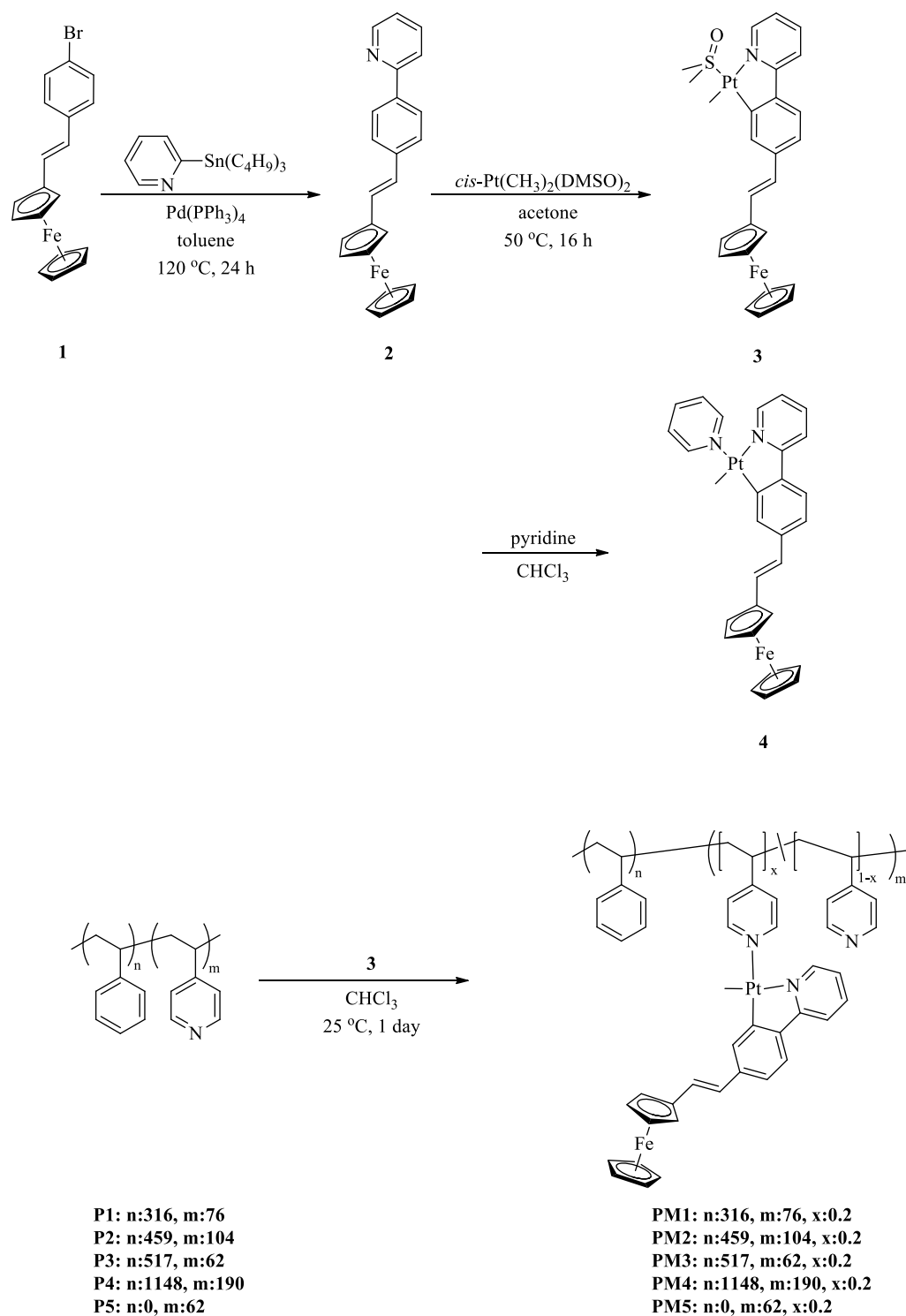
Scheme 1. Synthetic schemes for **PM1–PM5** and the model complex **4**.

All the polymers with a 0–40% loading of **3** were first studied by ^{1}H NMR spectroscopy

(Figure 2). After complexation of **3**, the 2 and 6 aromatic proton signals on the pyridine ring

gradually disappeared in the range of δ 8.10–8.50 ppm, whereas the aromatic and ferrocenyl

proton signals were detected at δ 7.40–7.90 and 4.00–4.60 ppm, respectively. Complexation of the metallic complex to P4VP was further confirmed by FTIR spectroscopy, TGA and TEM. Comparison of the IR spectra of **P2** with **PM2** in different loadings shows the disappearance of the uncomplexed PS-*b*-P4VP v_{C-N} band at 1415 cm^{-1} (Figure 3) and the decrease of signal intensity suggests the uptake of **3**. On the other hand, the peaks observed at 1471 and 1580 cm^{-1} correspond to the presence of the pyridine-coordinated complex **4**. The saturation loading of **3** was at about 30%, and further addition showed no change in the absorbance. Similar results were observed for the other three BCPs. The effect of complex loading on the morphology was explored through the thin film study.
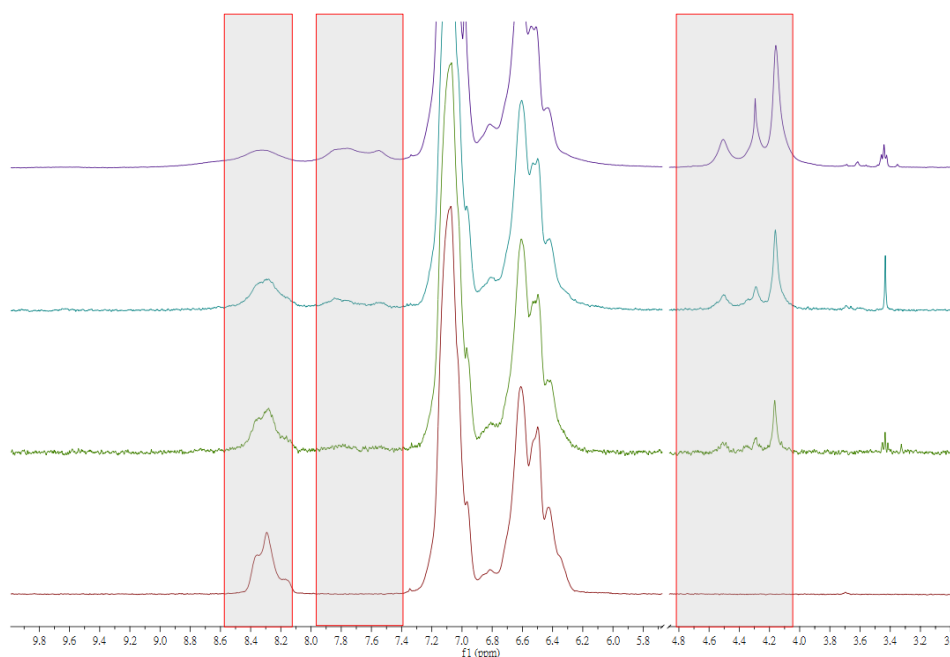
Figure 2. ^{1}H NMR spectra of **PM2** with x = 0, 0.1, 0.2 and 0.4 from the bottom to the top in CD$_2$Cl$_2$.
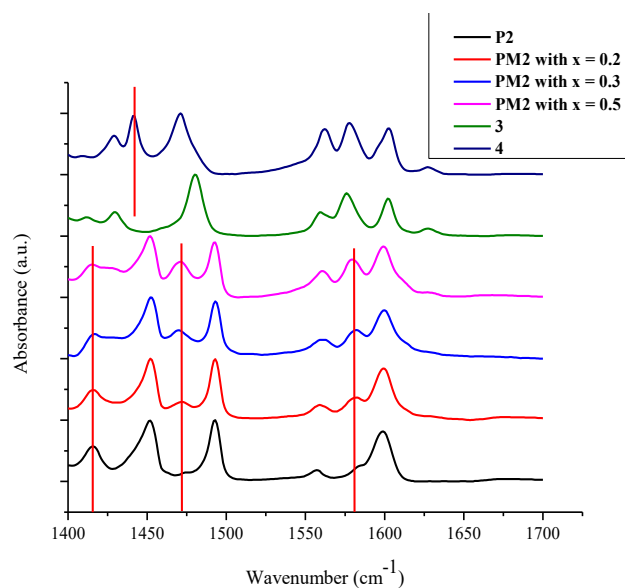
Figure 3. FTIR spectra of powder samples of **3**, **4** and **PM2** with x = 0, 0.2, 0.3 and 0.5.

Morphology characterization of PM1−PM4 in bulk and thin films. The phase separation

of these polymers in bulk and thin films was characterized by TEM and AFM, respectively. In

their TEM images (Figure 4), the darker domains in all cases were assigned to the electron-rich

P4VP-3 region (which contains the Fe and Pt atoms bounded with the **P4VP-3** block), while the

lighter domains were assigned to PS. The microtomed bulk film TEM images of **PM1−PM2** both

showed hexagonal-packed cylinders with a short range order, while some horizontally oriented

cylinders were also observed in the case of **PM1**. **PM3−PM4**, on the other hand, showed a

disordered spherical morphology.
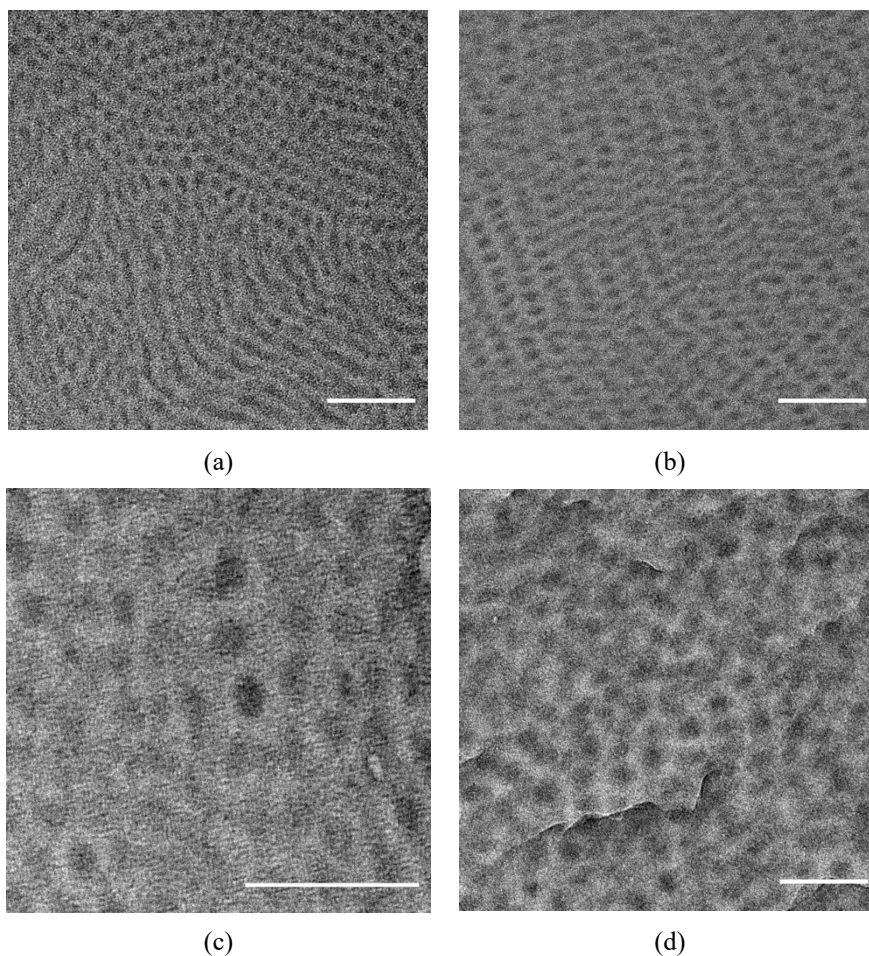
Figure 4. TEM images of microtomed samples of (a) **PM1**, (b) **PM2**, (c) **PM3** and (d) **PM4** (scale bar: 100 nm).

To further demonstrate the potential processability of **PM1−PM4**, thin films of these materials were formed from a chloroform solution, which is a good solvent for both blocks, *via* spin-coating at a rate of 3000 rpm onto a silicon wafer with a native oxide surface.[67-68] The concentration of polymer solution was varied from 0.3 to 1 wt% to adjust the film thickness, and 0.6 wt% was selected finally to yield a thickness of thin film in 30−50 nm as measured by AFM height profile. **PM2** was first chosen as a model to investigate the effect of different stoichiometric ratios (e.g. 0−90 %) of **3** on the morphological behavior in the thin films (Figure 5). A neat film of **P2** was immersed in ethanol prior to AFM analysis to increase the domain contrast *via* surface

reconstruction. Ethanol is a selective solvent for P4VP, which is insoluble for PS. This results in a porous structure by leaving the P4VP on the surface of thin film from the cylindrical channels, without changing the nanostructure.[69] Hence, it provides a height difference between the two BCP domains. The as-spun AFM height image showed vertically aligned cylinders, and further annealing in dioxane vapor allowed the order of the hexagonal-packing to be improved. This observation is consistent with the results mentioned by Russell et al.[70] By introducing **3** into **P2** with the loading percentage of 20–30%, both horizontally and vertically-aligned cylinders were observed. The quantity of horizontal cylinders was reduced when a 50% loading of **3** was used. A further increase to 70–90% in loading resulted in spherical dots without any cylindrical structures. As reported in the literature, small molecule-bound BCPs usually show composition-dependent morphological transitions.[41, 71-72] Such morphological changes are attributed to the increase in both density and volume fractions of the small molecule-bound P4VP block, which eventually alters the original position in the phase diagram (e.g. spherical to cylindrical and lamellar). However, there was no such expected morphological change in our case. Considering the IR results of **PM2**, the loading percentage of **3** reached the saturation level at around 30% and further addition of **3** did not result in coordination. These unbound complexes may aggregate themselves to promote the formation of ill-defined structures. Therefore, in order to maintain the desired morphology, 20% loading of the bimetallic complex was employed in these four polymers to ensure sufficient pyridine moieties for complexation.
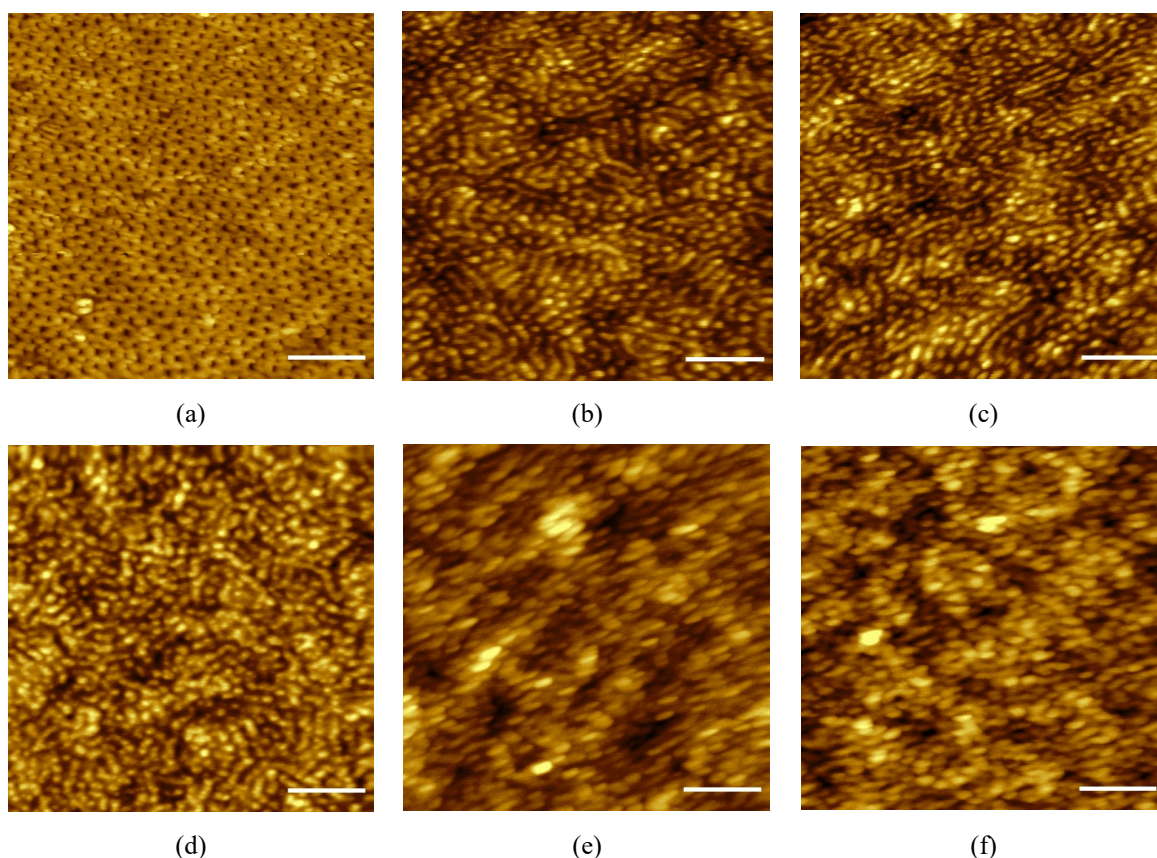
Figure 5. AFM height images of as-spun **PM2** on silicon wafers with (a) 0, (b) 20, (c) 30, (d) 50, (e) 70 and (f) 90% loading of complex **3** (scale bar: 200 nm).

The as-spun AFM height images of **PM1–PM4** films with a ca. 20 % loading of complex are illustrated in Figure 6, which are in agreement with their morphologies determined by TEM. The domain sizes were found to be slightly larger than those in the bulk state, which are attributed to the tip deconvolution effects (in which the resolution in AFM is partially lost). In the cases of both **PM1** and **PM2**, both horizontally- and vertically-aligned cylinders were observed with small amounts of hexagonal packing between the vertically-aligned cylinders. The random orientation of cylinders is believed to be kinetically trapped during the rapid spin-coating process, and additional processing (e.g. solvent annealing) was required to further improve the order and packing of the polymers. For **PM3** and **PM4**, disordered spheres were observed in their AFM images.
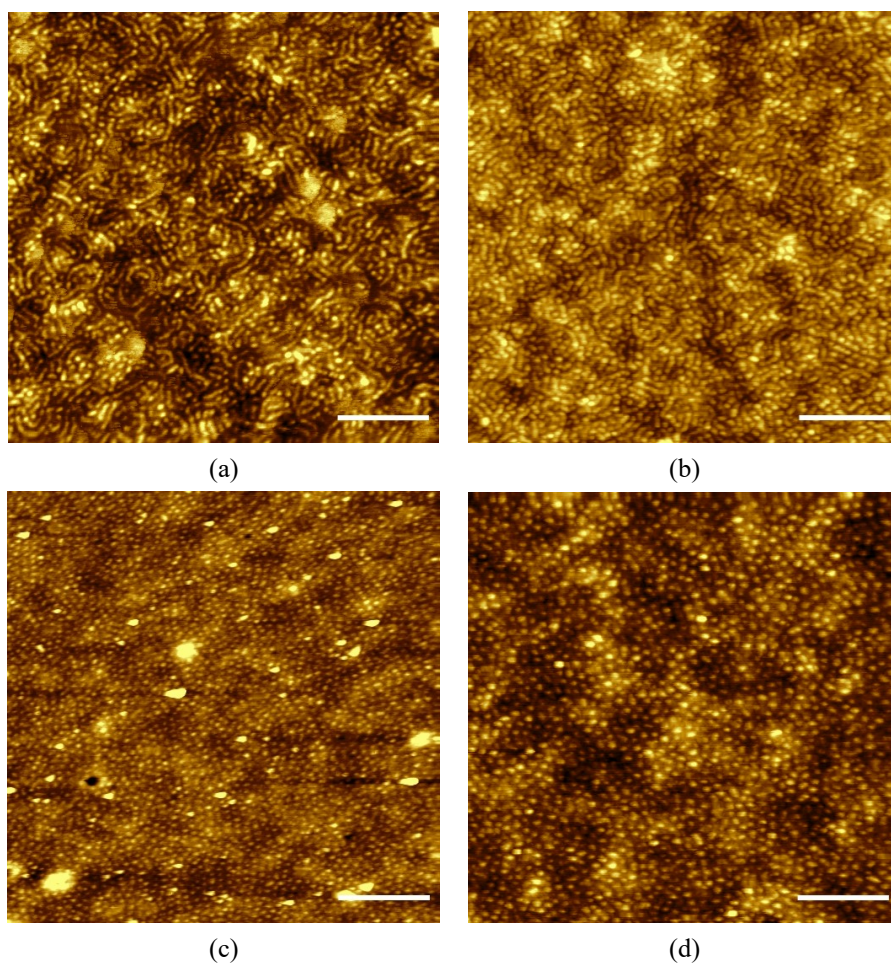
Figure 6. AFM height images of as-spun (a) **PM1**, (b) **PM2**, (c) **PM3** and (d) **PM4** with a ca. 20 % loading of complex **3** on silicon wafers (scale bar: 400 nm).

PM2 and **PM3** were chosen for further study. Both thermal and solvent annealing were performed for each polymer to investigate whether any improvement in their thin film morphology could be achieved. In the case of thermal annealing at 120 °C under vacuum for 1 day, no observable change in morphology was apparent. On the other hand, solvent-vapor annealing with dioxane (which is a selective solvent to PS block) was also investigated. In the as-spun thin film of **PM2**, both cylinders parallel and perpendicular to the substrate surface were observed, together with partial hexagonal packing as previously noted (Figure S1). After exposure to dioxane for 24 h, the striped patterns partially disappeared and some hexagonally arranged spheres were observed.

However, no improvement in packing was indicated for longer solvent exposure. This annealing result is quite different from that of neat **P2**, in which only ordered hexagonally-packed cylinders were observed after 24 h of dioxane exposure. We suggest that the complexation may hinder the mobility of the polymer chains to certain extent, which results in insufficient driving force to reach the same morphology as in the neat, complex-free polymer.[73] Similar results were obtained if a common solvent, chloroform, was employed. In the as-spun film of the sphere-forming **PM3**, no long-range order was displayed, while the dioxane-annealed film exhibited slight improvement in the packing of the spheres (Figure S2). Again, changing the solvent to chloroform resulted in no observable change of the as-spun film.

Pyrolysis studies of PM1–PM4 in bulk and thin film. To investigate the potential of **PM1–PM4** towards the formation of FePt NPs, thermolysis of these materials in bulk was first monitored by TGA at a scan rate of 10 °C/min under an atmosphere of nitrogen up to 800 °C (Figure S3). All the polymers were found to be thermally stable to weight loss below 300 °C. Charred black powders were formed after analysis. From the ceramic yield data, it appears that an appreciable portion of the organic component may remain inside the residue powder as amorphous carbonaceous matrix encapsulating the NPs (Table 2).

Table 2. Experimental and theoretical ceramic yields of **PM1-PM4** after pyrolysis.

	Experimental ceramic yield	**Theoretical ceramic yield[a]**
PM1	8.3%	7.4%
PM2	15.6%	7.0%
PM3	4.4%	4.5%
PM4	10.4%	5.8%

[a] Assuming only Fe and Pt atoms remained after pyrolysis.

The ceramic products were then imaged by TEM to obtain the average size of NPs. The average particle sizes of NPs were in the range of 4–8 nm (Figure S4 & Table 3). Under the same loading percentage of bimetallic complex **3**, the cylindrical BCPs (**PM1** and **PM2**) generally generate FePt NPs with larger size than those found in spherical BCPs (**PM3** and **PM4**), irrespective to the molecular weight. It is probably due to the fact that larger nanodomains are available in cylinder-forming BCPs than for their spherical analogues, allowing larger NPs to form. The Fe to Pt atomic ratio was calculated from EDX and the ratios are close to 1:1 in all cases. The formation of the *fct* $L1_0$ phase of the NPs was confirmed by the XRD patterns with the presence of (001) and (110) lattice peaks (Figures 7a and b).
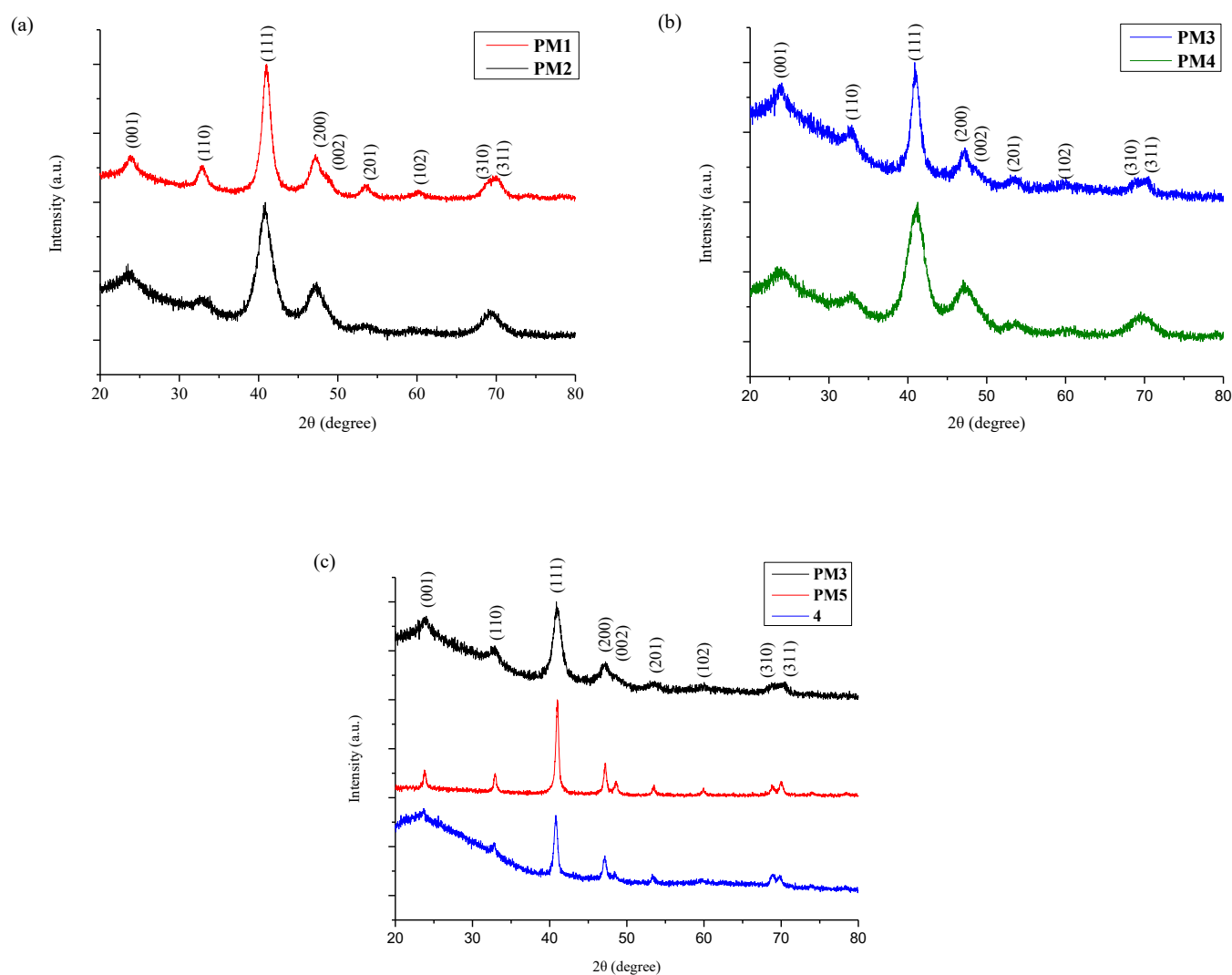
Figure 7. XRD patterns of the pyrolyzed samples of (a) **PM1** and **PM2**, (b) **PM3** and **PM4**, and (c) **PM3**, **PM5** and **4**.

To investigate the role of the BCP for NP growth, the pyrolysis behavior of **PM3** was compared to the corresponding P4VP homopolymer (**PM5**) at the same metal complex loading and also the model bimetallic complex **4**. Although the ceramic products obtained from the homopolymer and organometallic complex were confirmed to be *fct*-FePt NPs (Figure 7c), their sizes were around 3 times larger than those obtained from **PM3** (Figure 8 and the higher magnification images in Figure S5) (Table 3). This may be attributed to the phase-separation of the

BCP in bulk, in which the PS block effectively acts as a barrier to confine the NP growth. This is also supported by the larger standard deviation of the nanoparticle size in both cases of **PM5** and **4**. On the other hand, the Fe to Pt atomic ratio is found to be about 1:1.7, which shows a larger deviation from the targeted 1:1 ratio. Such deviation may be attributed to the lack of confinement.

To provide further evidence that the nanostructuring provided by the BCP is critical to achieving small FePt NPs with the desired stoichiometry, the pyrolysis of a blend of **4** or **PM5** with PS (in similar ratio to **PM3**) was performed. Similar fct-FePt NPs were obtained in these two cases, as confirmed by XRD (Figure S6). Interestingly, blending of PS with **PM5** resulted in a similar Fe to Pt atomic ratio as that of **PM3**, however, the size of NPs was found to be 3 times larger than those obtained from **PM3** (Figure S7a). These results eliminate the possibility that the sole presence of PS can act as a sufficient barrier to uncontrolled particle growth and indicate that the use of a nanostructured BCP is essential. This successfully demonstrated the importance of using a phase-separated BCP in the synthesis of FePt NPs, in order to achieve a smaller average NP size and a close to 1:1 Fe:Pt atomic ratio, which cannot be achieved by using homopolymer or the analogous molecular organometallic complex.

It is well-known that the high temperatures used in pyrolysis usually yield aggregated metallic NPs,[74-75] therefore inorganic materials (i.e. MgO, SiO_2 and NaCl) were commonly employed as barriers.[76-78] In contrast, it has been reported that the part of the polymer backbone can be converted to carbonaceous matrix, which suppressed the NP agglomeration, upon high

temperature pyrolysis.[23, 30, 49, 57] In the present study, self-assembly of bimetallic BCPs resulted in a nanostructured morphology which confined the bimetallic precursors within the P4VP domains. Upon the annealing, both Fe and Pt atoms were released from the polymer chains, and the carbonaceous matrix created by the PS block limited the diffusion of the metal atoms. As a result, NP fusion was greatly suppressed by the presence of surrounding carbonaceous matrix in the case of nanostructured **PM1-PM4**. However, in the case of **PM5** and **4**, there was no nanostructure confinement, which resulted in uncontrolled growth of NPs. Hence, larger NPs sizes with broader standard deviation were obtained.

(a)   (b)   (c)
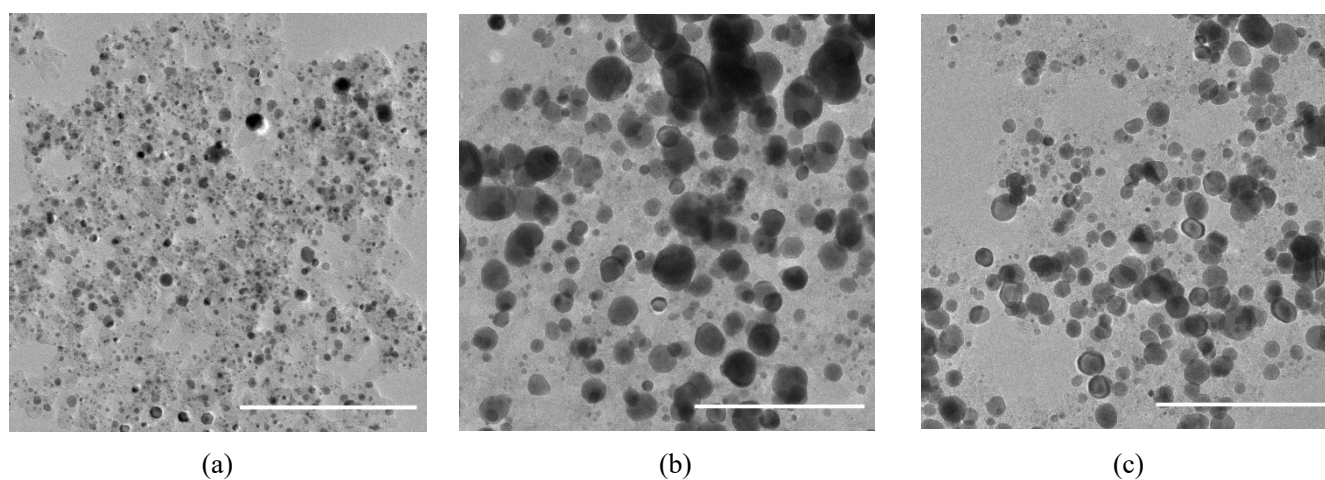
Figure 8. TEM images of pyrolyzed bulk samples of (a) **PM3**, (b) **PM5** and (c) **4** (scale bar = 200 nm).

Table 3. TEM, EDX and AFM data of block copolymers **PM1-PM4,** homopolymer **PM5** and the molecular complex **4**.

	Average NP size (nm) (SD[a])[b]	Fe:Pt atomic ratio[c]	Domain size in bulk (diameter, nm)[d]	Domain size in as-spun thin film (diameter, nm)[e]
PM1	5.9 (1.7)	0.47:0.53	12	18
PM2	7.6 (2.0)	0.57:0.43	21	23

PM3	5.5 (2.1)	0.44:0.56	20[f]	21
PM4	3.7 (0.9)	0.58:0.42	27	33
PM5	19.2 (7.3)	0.41:0.59	-	-
4	17.1 (6.9)	0.37:0.63	-	-
PS+PM5	18.5 (7.6)	0.44:0.56	-	-
PS+4	18.2 (8.5)	0.30:0.70	-	-

[a] SD: standard deviation.

[b] Determined from average value for >100 nanoparticles in the TEM images of pyrolyzed bulk samples.

[c] Ratio obtained from EDX, uncertainties of Fe and Pt were 0.02–0.06% and 0.08–0.17%, respectively.

[d] Determined from average value for >90 domains in the TEM images of microtomed samples.

[e] Determined from average value for >50 domains in the AFM height images of as-spun thin films.

[f] Determined from average value for >20 domains in the TEM images of microtomed samples.

The magnetic properties of the NPs obtained from **PM1−PM4** were characterized by the magnetic hysteresis loops at 300 K with a magnetic field up to 9 T (Figures 9 and S8). Taking **PM3** as an example, its coercivity was measured to be 8.69 kOe. The hysteresis loop is consistent to the XRD data in all the cases, showing the ferromagnetic nature of our *fct*-FePt NPs.
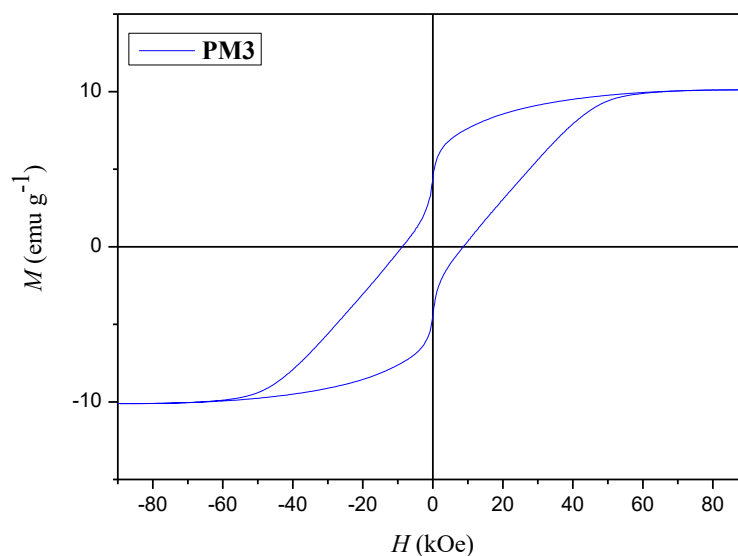
Figure 9. Magnetic hysteresis loop of the NPs from the pyrolyzed samples of **PM3** measured at 300 K.

In the introduction, an ideal schematic figure describing the concept of the formation of large area of FePt NPs by solely using a thin film of bimetallic-containing BCP was given (Figure 1). Although the attempt to achieve long-range order in thin film was not successful at this stage, it was still useful to investigate the effect of pyrolysis on the thin film. The thin films were directly pyrolyzed to 800 °C at a ramp temperature of 10 °C/min in 5% H_2/Ar. The samples were then analyzed by AFM. In the case of **PM3**, the spherical features were observed in both as-spun and annealed films after pyrolysis, but suffered from the lack of order (Figures 10c and d). With regard to the size, there are no significant differences before and after pyrolysis (ca. 18–22 nm), which may suggest no or little coalescence during pyrolysis. Similar results were observed in the case of **PM2** (Figures 10a and b). Interestingly, horizontally-aligned cylinders were observed in the as-spun thin film before pyrolysis, but only spherical shaped ceramic materials were detected after pyrolysis by AFM analysis. In the case of **PM3**, if the pyrolysis condition could be further optimized to retain the order of spherical morphology, this prototype BPM should provide an areal density of 400 Gb in^{-2} (calculated from the as-spun thin film). Further optimization of this BCP system to provide the crosslinking is necessary to facilitate the morphology retention[30] and work along this line is currently in progress.
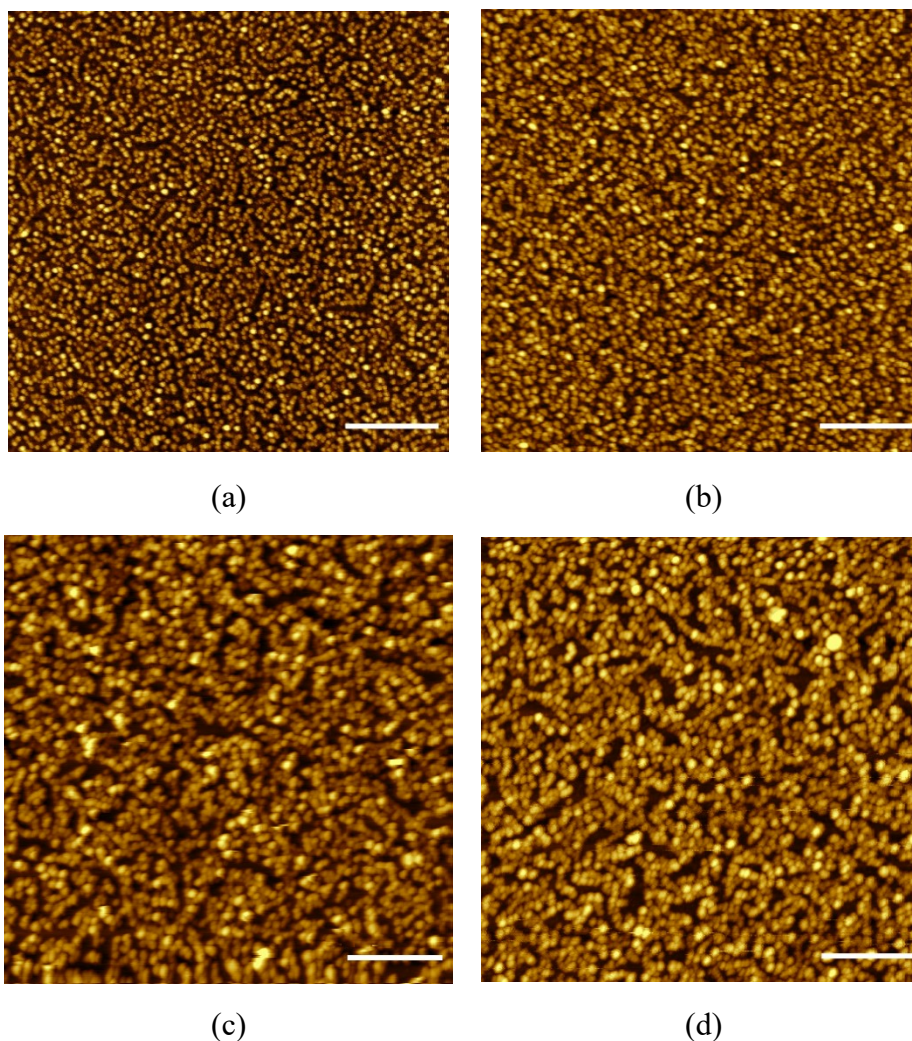
Figure 10. AFM height images of pyrolyzed **PM2** with (a) as-spun and (b) 24 h of dioxane exposure and that of **PM3** with (c) as-spun and (d) 24 h of dioxane exposure on silicon wafers (scale bar: 400 nm)

CONCLUSION

In this study, arrays of FePt NPs were prepared from metallo-BCP templating. To achieve this goal, bimetallic complex **3** was designed to facilitate the coordination linkage to the pyridine unit in PS-*b*-P4VP, so as to create phase-separated cylindrical or spherical FePt-containing nanodomains. A 20% loading of pyridine ligands in the BCPs was targeted to ensure efficient metal binding and well-characterized morphology in thin films.

Thin film self-assembly was conducted in **PM2** and **PM3** to illustrate the capability of these polymers as precursor to form spatially isolated FePt NPs in the well order. The corresponding morphology found in bulk state was found to be reproducible in the thin films. After solvent-vapor annealing in dioxane, slightly improved hexagonally-packed cylindrical and spherical morphologies were revealed. However, the packing was not as good as for the precursor PS-*b*-P4VP BCP, which may probably be due to the decrease in mobility after complexation. The pyrolysis of bulk samples at 800 °C under an inert atmosphere yielded *fct*-FePt NPs with average particle size of 4–8 nm, which was confirmed by TEM and XRD. EDX showed nearly 1:1 Fe to Pt atomic ratio. From these results, the importance of using metal-containing BCPs in the synthesis of FePt NPs was demonstrated in order to achieve smaller average NP size with nearly 1:1 Fe:Pt atomic ratio. In thin film, the features were retained during pyrolysis for **PM2** and **PM3**, but they did not show high order. The size of the FePt-containing domain was similar to that before pyrolysis, which showed no or little coalescence after pyrolysis. To optimize the pyrolysis condition in our BCP system, UV-irradiation may be required in the future study to allow better shape retention during pyrolysis.[30]

From the above results, metallo-BCP lithography is proved to be an effective and coalescence-free approach to convert a single bimetallic source into FePt NPs without the need of surfactants of weak binding strength or complicated addition sequence of monometallic salts.

ACKNOWLEDGEMENTS

SUPPORTING INFORMATION

Additional AFM (Figures S1 and S2) and TEM images (Figures S4, S5 and S7), TGA traces (Figure S3), XRD spectrum (Figure S6), Magnetic hysteresis loops (Figure S8), ^{1}H NMR spectra (Figures S9–S11), MALDI-TOF mass spectra (Figures S12–S14) and EDX analysis plots (Figures S15–S17).

REFERENCES

1.   Hardy, C. G.; Zhang, J.; Yan, Y.; Ren, L.; Tang, C. Metallopolymers with Transition Metals in the Side-Chain by Living and Controlled Polymerization Techniques. *Prog. Polym. Sci.* **2014,** *39*, 1742−1796.

2.   Nunns, A.; Gwyther, J.; Manners, I. Inorganic Block Copolymer Lithography. *Polymer* **2013,** *54*, 1269−1284.

3.   Whittell, G. R.; Hager, M. D.; Schubert, U. S.; Manners, I. Functional Soft Materials from Metallopolymers and Metallosupramolecular Polymers. *Nat. Mater.* **2011,** *10*, 176−188.

4.   Ho, C.-L.; Yu, Z.-Q.; Wong, W.-Y. Multifunctional Polymetallaynes: Properties, Functions and Applications. *Chem. Soc. Rev.* **2016,** *45*, 5264−5295.

5.   Pietschnig, R. Polymers with Pendant Ferrocenes. *Chem. Soc. Rev.* **2016,** *45*, 5216−5231.

6.   Gallei, M.; Rüttiger, C. Recent Trends in Metallopolymer Design: Redox-Controlled Surfaces, Porous Membranes, and Switchable Optical Materials Using Ferrocene-Containing Polymers. *Chem. Eur. J.* **2018,** *24*, 10006−10021.

7.   Yan, Y.; Zhang, J.; Ren, L.; Tang, C. Metal-Containing and Related Polymers for Biomedical Applications. *Chem. Soc. Rev.* **2016,** *45*, 5232−5263.

8.   Feng, X.; Zhang, K.; Hempenius, M. A.; Vancso, G. J. Organometallic Polymers for Electrode Decoration in Sensing Applications. *RSC Adv.* **2015,** *5*, 106355−106376.

9.   Zhang, K.; Feng, X.; Ye, C.; Hempenius, M. A.; Vancso, G. J. Hydrogels with a Memory: Dual-Responsive, Organometallic Poly(ionic liquid)s with Hysteretic Volume-Phase Transition. *J. Am. Chem. Soc.* **2017,** *139*, 10029−10035.

10.   Ho, C.-L.; Wong, W.-Y. Metal-Containing Polymers: Facile Tuning of Photophysical Traits and Emerging Applications in Organic Electronics and Photonics. *Coord. Chem. Rev.* **2011,** *255*, 2469–2502.

11.   Xiang, J.; Ho, C.-L.; Wong, W.-Y. Metallopolymers for Energy Production, Storage and Conservation. *Polym. Chem.* **2015,** *6*, 6905–6930.

12.   Marin, V.; Holder, E.; Hoogenboom, R.; Schubert, U. S. Functional Ruthenium(II)- and Iridium(III)-Containing Polymers for Potential Electro-Optical Applications. *Chem. Soc. Rev.* **2007,** *36*, 618–635.

13.   Rabiee Kenaree, A.; Gilroy, J. B. Synthesis and Characterization of Metal-Rich Phosphonium Polyelectrolytes and Their Use as Precursors to Nanomaterials. *Dalton Trans.* **2016,** *45*, 18229–18240.

14.   MacLachlan, M. J.; Ginzburg, M.; Coombs, N.; Raju, N. P.; Greedan, J. E.; Ozin, G. A.; Manners, I. Superparamagnetic Ceramic Nanocomposites: Synthesis and Pyrolysis of Ring-Opened Poly(ferrocenylsilanes) inside Periodic Mesoporous Silica. *J. Am. Chem. Soc.* **2000,** *122*, 3878–3891.

15.   Ginzburg, M.; MacLachlan, M. J.; Yang, S. M.; Coombs, N.; Coyle, T. W.; Raju, N. P.; Greedan, J. E.; Herber, R. H.; Ozin, G. A.; Manners, I. Genesis of Nanostructured, Magnetically Tunable Ceramics from the Pyrolysis of Cross-Linked Polyferrocenylsilane Networks and Formation of Shaped Macroscopic Objects and Micron Scale Patterns by Micromolding inside Silicon Wafers. *J. Am. Chem. Soc.* **2002,** *124*, 2625–2639.

16.   Zhang, J.; Yan, Y.; Chance, M. W.; Chen, J.; Hayat, J.; Ma, S.; Tang, C. Charged Metallopolymers as Universal Precursors for Versatile Cobalt Materials. *Angew. Chem. Int. Ed.* **2013,** *52*, 13387–13391.

17.   Dong, Q.; Meng, Z.; Ho, C.-L.; Guo, H.; Yang, W.; Manners, I.; Xu, L.; Wong, W.-Y. A Molecular Approach to Magnetic Metallic Nanostructures from Metallopolymer Precursors. *Chem. Soc. Rev.* **2018,** *47*, 4934–4953.

18. Yiu, S.-C.; Ho, C.-L.; Wong, W.-Y., Nanopatterning of Functional Metallopolymers via Top-Down Approach. In

Polymer-Engineered Nanostructures for Advanced Energy Applications, Lin, Z., Yang, Y., Zhang, A., Eds. Springer

International Publishing: Cham, 2017; pp 51−70.

19. Ramanathan, M.; Darling, S. B. Nanofabrication with Metallopolymers - Recent Developments and Future

Perspectives. *Polym. Int.* **2013,** *62*, 1123−1134.

20. Ramanathan, M.; Tseng, Y.-C.; Ariga, K.; Darling, S. B. Emerging Trends in Metal-Containing Block

Copolymers: Synthesis, Self-Assembly, and Nanomanufacturing Applications. *J. Mater. Chem. C* **2013,** *1*, 2080−2091.

21. Korczagin, I.; Lammertink, R. G. H.; Hempenius, M. A.; Golze, S.; Vancso, G. J., Surface Nano- and

Microstructuring with Organometallic Polymers. In *Ordered Polymeric Nanostructures at Surfaces*, Vancso, G. J., Ed.

Springer Berlin Heidelberg: Berlin, Heidelberg, 2006; pp 91−117.

22. Wang, X.; McHale, R. Metal-Containing Polymers: Building Blocks for Functional (Nano)Materials. *Macromol.

Rapid Commun.* **2010,** *31*, 331−350.

23. Dong, Q.; Li, G.; Ho, C.-L.; Faisal, M.; Leung, C.-W.; Pong, P. W.-T.; Liu, K.; Tang, B.-Z.; Manners, I.; Wong,

W.-Y. A Polyferroplatinyne Precursor for the Rapid Fabrication of L1$_0$-FePt-type Bit Patterned Media by Nanoimprint

Lithography. *Adv. Mater.* **2012,** *24*, 1034−1040.

24. Meng, Z.; Li, G.; Ng, S.-M.; Wong, H.-F.; Yiu, S.-C.; Ho, C.-L.; Leung, C.-W.; Wong, W.-Y. Nanopatterned

L1$_0$-FePt Nanoparticles from Single-Source Metallopolymer Precursors for Potential Application in Ferromagnetic

Bit-Patterned Media Magnetic Recording. *Polym. Chem.* **2016,** *7*, 4467−4475.

25. Cheng, J. Y.; Ross, C. A.; Chan, V. Z.-H.; Thomas, E. L.; Lammertink, R. G. H.; Vancso, G. J. Formation of a

Cobalt Magnetic Dot Array via Block Copolymer Lithography. *Adv. Mater.* **2001,** *13*, 1174–1178.

26.   Yoo, S. I.; Sohn, B.-H.; Zin, W.-C.; An, S.-J.; Yi, G.-C. Self-Assembled Arrays of Zinc Oxide Nanoparticles from Monolayer Films of Diblock Copolymer Micelles. *Chem. Commun.* **2004,** 2850–2851.

27.   Li, X.; Lau, K. H. A.; Kim, D. H.; Knoll, W. High-Density Arrays of Titania Nanoparticles Using Monolayer Micellar Films of Diblock Copolymers as Templates. *Langmuir* **2005,** *21*, 5212–5217.

28.   Zhou, J.; Whittell, G. R.; Manners, I. Metalloblock Copolymers: New Functional Nanomaterials. *Macromolecules* **2014,** *47*, 3529–3543.

29.   Hinderling, C.; Keles, Y.; Stöckli, T.; Knapp, H. F.; de los Arcos, T.; Oelhafen, P.; Korczagin, I.; Hempenius, M. A.; Vancso, G. J.; Pugin, R.; Heinzelmann, H. Organometallic Block Copolymers as Catalyst Precursors for Templated Carbon Nanotube Growth. *Adv. Mater.* **2004,** *16*, 876–879.

30.   Rider, D. A.; Liu, K.; Eloi, J.-C.; Vanderark, L.; Yang, L.; Wang, J.-Y.; Grozea, D.; Lu, Z.-H.; Russell, T. P.; Manners, I. Nanostructured Magnetic Thin Films from Organometallic Block Copolymers: Pyrolysis of Self-Assembled Polystyrene-*block*-poly(ferrocenylethylmethylsilane). *ACS Nano* **2008,** *2*, 263–270.

31.   Hardy, C. G.; Ren, L.; Ma, S.; Tang, C. Self-Assembly of Well-Defined Ferrocene Triblock Copolymers and Their Template Synthesis of Ordered Iron Oxide Nanoparticles. *Chem. Commun.* **2013,** *49*, 4373–4375.

32.   Lu, J. Q.; Kopley, T. E.; Moll, N.; Roitman, D.; Chamberlin, D.; Fu, Q.; Liu, J.; Russell, T. P.; Rider, D. A.; Manners, I. High-Quality Single-Walled Carbon Nanotubes with Small Diameter, Controlled Density, and Ordered Locations Using a Polyferrocenylsilane Block Copolymer Catalyst Precursor. *Chem. Mater.* **2005,** *17*, 2227–2231.

33.   Rider, D. A.; Cavicchi, K. A.; Power-Billard, K. N.; Russell, T. P.; Manners, I. Diblock Copolymers with

Amorphous Atactic Polyferrocenylsilane Blocks: Synthesis, Characterization, and Self-Assembly of Polystyrene-*block*-poly(ferrocenylethylmethylsilane) in the Bulk State. *Macromolecules* **2005,** *38*, 6931−6938.

34. Rider, D. A.; Cavicchi, K. A.; Vanderark, L.; Russell, T. P.; Manners, I. Orientationally Controlled Nanoporous Cylindrical Domains in Polystyrene-*b*-poly(ferrocenylethylmethylsilane) Block Copolymer Films. *Macromolecules* **2007,** *40*, 3790−3796.

35. Al-Kharusi, H. N.; Wu, L.; Whittell, G.; Harniman, R.; Manners, I. Synthesis, Thin-film Self-Assembly, and Pyrolysis of Ruthenium-Containing Polyferrocenylsilane Block Copolymers. *Polym. Chem.* **2018,** *9*, 2951−2963.

36. Jiang, B.; Nykypanchuk, D.; Endoh, M. K.; Chen, X.; Qian, B.; Kisslinger, K.; Koga, T.; Parise, J. B.; Grubbs, R. B. Phase Behavior of Alkyne-Functionalized Styrenic Block Copolymer/Cobalt Carbonyl Adducts and *in Situ* Formation of Magnetic Nanoparticles by Thermolysis. *Macromolecules* **2016,** *49*, 853−865.

37. Mîinea, L. A.; Sessions, L. B.; Ericson, K. D.; Glueck, D. S.; Grubbs, R. B. Phenylethynylstyrene−Cobalt Carbonyl Block Copolymer Composites. *Macromolecules* **2004,** *37*, 8967−8972.

38. Al-Badri, Z. M.; Maddikeri, R. R.; Zha, Y.; Thaker, H. D.; Dobriyal, P.; Shunmugam, R.; Russell, T. P.; Tew, G. N. Room Temperature Magnetic Materials from Nanostructured Diblock Copolymers. *Nat. Commun.* **2011,** *2*, 482.

39. Hadadpour, M.; Ragogna, P. J. Nanopatterning and Micropatterning of Cobalt Containing Block Copolymers via Phase-Separation and Lithographic Techniques. *J. Polym. Sci., Part A: Polym. Chem.* **2015,** *53*, 2747−2754.

40. Rüttiger, C.; Pfeifer, V.; Rittscher, V.; Stock, D.; Scheid, D.; Vowinkel, S.; Roth, F.; Didzoleit, H.; Stühn, B.; Elbert, J.; Ionescu, E.; Gallei, M. One for All: Cobalt-Containing Polymethacrylates for Magnetic Ceramics, Block Copolymerization, Unexpected Electrochemistry, and Stimuli- Responsiveness. *Polym. Chem.* **2016,** *7*, 1129−1137.

41.   Davidi, I.; Patra, D.; Hermida-Merino, D.; Portale, G.; Rotello, V. M.; Raviv, U.; Shenhar, R. Hierarchical

Structures of Polystyrene-*block*-poly(2-vinylpyridine)/Palladium–Pincer Surfactants: Effect of Weak Surfactant–

Polymer Interactions on the Morphological Behavior. *Macromolecules* **2014,** *47*, 5774–5783.

42.   Davidi, I.; Shenhar, R. Synthesis of Disk-Shaped Nanoparticle Aggregates Organized in Hierarchical Structures

in Block Copolymer Matrices. *Polymer* **2015,** *64*, 39–45.

43.   Weller, D.; Moser, A.; Folks, L.; Best, M. E.; Wen, L.; Toney, M. F.; Schwickert, M.; Thiele, J. U.; Doerner, M.

F. High K_u Materials Approach to 100 Gbits/in^2. *IEEE Trans. Magn.* **2000,** *36*, 10–15.

44.   Weller, D.; Doerner, M. F. Extremely High-Density Longitudinal Magnetic Recording Media. *Annu. Rev. Mater.*

Sci. **2000,** *30*, 611–644.

45.   Farrow, R. F. C.; Weller, D.; Marks, R. F.; Toney, M. F.; Cebollada, A.; Harp, G. R. Control of the Axis of

Chemical Ordering and Magnetic Anisotropy in Epitaxial FePt Films. *J. Appl. Phys.* **1996,** *79*, 5967–5969.

46.   Chen, W.; Kim, J.; Sun, S.; Chen, S. Electro-Oxidation of Formic Acid Catalyzed by FePt Nanoparticles. *Phys.*

Chem. Chem. Phys. **2006,** *8*, 2779–2786.

47.   Kim, J.; Lee, Y.; Sun, S. Structurally Ordered FePt Nanoparticles and Their Enhanced Catalysis for Oxygen

Reduction Reaction. *J. Am. Chem. Soc.* **2010,** *132*, 4996–4997.

48.   Andreas, M.; Kentaro, T.; David, T. M.; Manfred, A.; Yoshiaki, S.; Yoshihiro, I.; Shouheng, S.; Eric, E. F.

Magnetic Recording: Advancing into the Future. *J. Phys. D: Appl. Phys.* **2002,** *35*, R157.

49.   Liu, K.; Ho, C.-L.; Aouba, S.; Zhao, Y.-Q.; Lu, Z.-H.; Petrov, S.; Coombs, N.; Dube, P.; Ruda, H. E.; Wong,

W.-Y.; Manners, I. Synthesis and Lithographic Patterning of FePt Nanoparticles Using a Bimetallic Metallopolyyne

Precursor. *Angew. Chem. Int. Ed.* **2008,** *47*, 1255–1259.

50.   Meng, Z.; Li, G.; Wong, H.-F.; Ng, S.-M.; Yiu, S.-C.; Ho, C.-L.; Leung, C.-W.; Manners, I.; Wong, W.-Y. Patterning of L1$_0$ FePt Nanoparticles with Ultra-High Coercivity for Bit-Patterned Media. *Nanoscale* **2017,** *9*, 731–738.

51.   Li, G.; Dong, Q.; Xin, J.; Leung, C. W.; Lai, P. T.; Wong, W.-Y.; Pong, P. W. T. Patterning Micro- and Nano-Structured FePt by Direct Imprint Lithography. *Microelectron. Eng.* **2013,** *110*, 192–197.

52.   Kim, K.-S.; Kim, J.-H.; Lee, H.-J.; Lee, S.-R. Tribology Issues in Nanoimprint Lithography. *J. Mech. Sci. Technol.* **2010,** *24*, 5–12.

53.   Aissou, K.; Fleury, G.; Pecastaings, G.; Alnasser, T.; Mornet, S.; Goglio, G.; Hadziioannou, G. Hexagonal-to-Cubic Phase Transformation in Composite Thin Films Induced by FePt Nanoparticles Located at PS/PEO Interfaces. *Langmuir* **2011,** *27*, 14481–14488.

54.   Basly, B.; Alnasser, T.; Aissou, K.; Fleury, G.; Pecastaings, G.; Hadziioannou, G.; Duguet, E.; Goglio, G.; Mornet, S. Optimization of Magnetic Inks Made of L1$_0$-Ordered FePt Nanoparticles and Polystyrene-*block*-Poly(ethylene oxide) Copolymers. *Langmuir* **2015,** *31*, 6675–6680.

55.   Schelhas, L. T.; Farrell, R. A.; Halim, U.; Tolbert, S. H. Directed Self-Assembly as a Route to Ferromagnetic and Superparamagnetic Nanoparticle Arrays. *Adv. Funct. Mater.* **2014,** *24*, 6956–6962.

56.   Gao, Y.; Zhang, X.; Yin, Z.; Qu, S.; You, J.; Chen, N. Magnetic Properties of FePt Nanoparticles Prepared by a Micellar Method. *Nanoscale Res. Lett.* **2009,** *5*, 1–6.

57.   Kang, E.; Jung, H.; Park, J.-G.; Kwon, S.; Shim, J.; Sai, H.; Wiesner, U.; Kim, J. K.; Lee, J. Block Copolymer

Directed One-Pot Simple Synthesis of $L1_0$-Phase FePt Nanoparticles inside Ordered Mesoporous Aluminosilicate/Carbon Composites. *ACS Nano* **2011,** *5*, 1018−1025.

58. Siani, A.; Captain, B.; Alexeev, O. S.; Stafyla, E.; Hungria, A. B.; Midgley, P. A.; Thomas, J. M.; Adams, R. D.; Amiridis, M. D. Improved CO Oxidation Activity in the Presence and Absence of Hydrogen over Cluster-Derived PtFe/SiO$_2$ Catalysts. *Langmuir* **2006,** *22*, 5160−5167.

59. Song, H. M.; Hong, J. H.; Lee, Y. B.; Kim, W. S.; Kim, Y.; Kim, S.-J.; Hur, N. H. Growth of FePt Nanocrystals by a Single Bimetallic Precursor [(CO)$_3$Fe(μ-dppm)(μ-CO)PtCl$_2$]. *Chem. Commun.* **2006,** 1292−1294.

60. Chabanne, L.; Matas, I.; Patra, S. K.; Manners, I. Organic-Metalloblock Copolymers via Photocontrolled Anionic Ring-Opening Polymerization. *Polym. Chem.* **2011,** *2*, 2651−2660.

61. Erhard, M.; Lam, K.; Haddow, M.; Whittell, G. R.; Geiger, W. E.; Manners, I. Polyferrocenylsilane Homopolymers and Diblock Copolymers with Pendant Ruthenocenyl Groups by Photocontrolled Ring-Opening Polymerisation. *Polym. Chem.* **2014,** *5*, 1264−1274.

62. Zhang, J.; Yan, Y.; Chen, J.; Chance, W. M.; Hayat, J.; Gai, Z.; Tang, C. Nanostructured Metal/Carbon Composites from Heterobimetallic Block Copolymers with Controlled Magnetic Properties. *Chem. Mater.* **2014,** *26*, 3185−3190.

63. Price, J. H.; Williamson, A. N.; Schramm, R. F.; Wayland, B. B. Palladium(II) and Platinum(II) Alkyl Sulfoxide Complexes. Examples of Sulfur-Bonded, Mixed Sulfur- and Oxygen-Bonded, and Totally Oxygen-Bonded Complexes. *Inorg. Chem.* **1972,** *11*, 1280−1284.

64. Shin, D.; Switzer, C. A Metallo Base-Pair Incorporating a Terpyridyl-like Motif:

Bipyridyl-Pyrimidinone·Ag(I)·4-Pyridine. *Chem. Commun.* **2007**, 4401−4403.

65.   Eaborn, C.; Kundu, K.; Pidcock, A. Synthesis of Platinum(II) Alkyl and Aryl Complexes from $K_2[PtCl_4]$ and

Tetraorganotin Compounds in Dimethyl Sulphoxide. *J. Chem. Soc., Dalton Trans.* **1981**, 933−938.

66.   Shi, J.; Tong, B.; Li, Z.; Shen, J.; Zhao, W.; Fu, H.; Zhi, J.; Dong, Y.; Häussler, M.; Lam, J. W. Y.; Tang, B. Z.

Hyperbranched Poly(ferrocenylphenylenes): Synthesis, Characterization, Redox Activity, Metal Complexation,

Pyrolytic Ceramization, and Soft Ferromagnetism. *Macromolecules* **2007,** *40*, 8195−8204.

67.   Ye, X.; Niroomand, H.; Hu, S.; Khomami, B. Block Copolymer Micelle Formation in a Solvent Good for All the

Blocks. *Colloid. Polym. Sci.* **2015,** *293*, 2799−2805.

68.   Gowd, E. B.; Koga, T.; Endoh, M. K.; Kumar, K.; Stamm, M. Pathways of Cylindrical Orientations in

PS-*b*-P4VP Diblock Copolymer Thin Films upon Solvent Vapor Annealing. *Soft Matter* **2014,** *10*, 7753−7761.

69.   Park, S.; Kim, B.; Wang, J.-Y.; Russell, T. P. Fabrication of Highly Ordered Silicon Oxide Dots and Stripes from

Block Copolymer Thin Films. *Adv. Mater.* **2008,** *20*, 681−685.

70.   Park, S.; Wang, J.-Y.; Kim, B.; Xu, J.; Russell, T. P. A Simple Route to Highly Oriented and Ordered

Nanoporous Block Copolymer Templates. *ACS Nano* **2008**, *2*, 766−772.

71.   Ruokolainen, J.; Saariaho, M.; Ikkala, O.; ten Brinke, G.; Thomas, E. L.; Torkkeli, M.; Serimaa, R.

Supramolecular Routes to Hierarchical Structures: Comb-Coil Diblock Copolymers Organized with Two Length

Scales. *Macromolecules* **1999,** *32*, 1152−1158.

72.   Nandan, B.; Vyas, M. K.; Böhme, M.; Stamm, M. Composition-Dependent Morphological Transitions and

Pathways in Switching of Fine Structure in Thin Films of Block Copolymer Supramolecular Assemblies.

Macromolecules **2010,** *43*, 2463–2473.

73.   Etxeberria, H.; Fernandez, R.; Zalakain, I.; Mondragon, I.; Eceiza, A.; Kortaberria, G. Effect of CdSe

Nanoparticle Addition on Nanostructuring of PS-*b*-P4VP Copolymer via Solvent Vapor Exposure. *J. Colloid Interface*

Sci. **2014,** *416*, 25−29.

74.   Dai, Z. R.; Sun, S.; Wang, Z. L. Phase Transformation, Coalescence, and Twinning of Monodisperse FePt

Nanocrystals. *Nano Lett.* **2001,** *1*, 443-447.

75.   Elkins, K. E.; Vedantam, T. S.; Liu, J. P.; Zeng, H.; Sun, S.; Ding, Y.; Wang, Z. L. Ultrafine FePt Nanoparticles

Prepared by the Chemical Reduction Method. *Nano Lett.* **2003,** *3*, 1647−1649.

76.   Kim, J.; Rong, C.; Lee, Y.; Liu, J. P.; Sun, S. From Core/Shell Structured FePt/Fe3O4/MgO to Ferromagnetic

FePt Nanoparticles. *Chem. Mater.* **2008,** *20*, 7242−7245.

77.   Tamada, Y.; Yamamoto, S.; Takano, M.; Nasu, S.; Ono, T. Well-Ordered L10-FePt Nanoparticles Synthesized by

Improved SiO$_2$-Nanoreactor Method. *Appl. Phys. Lett.* **2007,** *90*, 162509.

78.   He, J.; Bian, B.; Zheng, Q.; Du, J.; Xia, W.; Zhang, J.; Yan, A.; Liu, J. P. Direct Chemical Synthesis of Well

Dispersed L10-FePt Nanoparticles with Tunable Size and Coercivity. *Green Chem.* **2016,** *18*, 417−422.